JBC Papers in Press. Published on March 21, 2012 as Manuscript M112.355818
The latest version is at http://www.jbc.org/cgi/doi/10.1074/jbc.M112.355818

The Substrate Selectivity of YgfU, a Uric Acid Transporter from *Escherichia coli**

Konstantinos Papakostas, and Stathis Frillingos

From the Laboratory of Biological Chemistry, University of Ioannina Medical School, Ioannina, Greece

*Running title: *Selectivity of transporter YgfU for uric acid*

To whom correspondence should be addressed: Stathis Frillingos, University of Ioannina Medical School, Laboratory of Biological Chemistry, 45110 Ioannina, Greece; e-mail: efriligo@cc.uoi.gr

Keywords: purine transport; evolution; uric acid; Cys-scanning data

Background: YgfU is homologous to nucleobase transporters of the ubiquitous family NCS2.
Results: YgfU transports uric acid. A single-amino acid replacement (T100A) converts YgfU to a dual-selectivity transporter for uric acid and xanthine.
Conclusion: Thr-100 is essential for the uric acid selectivity.
Significance: Dissecting selectivity determinants in family NCS2 is crucial for understanding evolution of purine uptake.

SUMMARY

The ubiquitous nucleobase-ascorbate transporter (NAT/NCS2) family includes more than 2,000 members but only 15 have been characterized experimentally. *Escherichia coli* has 10 members, of which functionally known are the uracil permease UraA and the xanthine permeases XanQ and XanP. Of the remaining members, YgfU is closely related in sequence and genomic locus with XanQ. We analyzed YgfU and showed that it is a proton-gradient dependent, low-affinity (K_m 0.5 mM) and high-capacity transporter for uric acid. It also shows a low capacity for transport of xanthine at 37° C but not at 25° C. Based on the set of positions delineated as important from our previous Cys-scanning analysis of permease XanQ, we subjected YgfU to rationally designed site-directed mutagenesis. The results show that the conserved His-37 (TM1), Glu-270 (TM8), Asp-298 (TM9), Gln-318 and Asn-319 (TM10) are functionally irreplaceable, and Thr-100 (TM3) is essential for the uric acid selectivity since its replacement with Ala allows efficient uptake of xanthine. The key role of these residues is corroborated by the conservation pattern and homology modeling on the recently described x-ray structure of permease UraA. In addition, site-specific replacements at TM8 (S271A, M274D, V282S) impair expression in the membrane, V320N (TM10) inactivates, and R327G (TM10) or S426N (TM14) reduces the affinity for uric acid (four-fold increased K_m). Our study shows that comprehensive analysis of structure-function relationships in a newly characterized transporter can be accomplished with relatively few site-directed replacements, based on the knowledge available from Cys-scanning mutagenesis of a prototypic homolog.

Conservation of sequence and overall structure in many evolutionarily broad families of transporters often correlates with high functional variations between homologs. In most cases, however, it is common that few of the members have been studied for structure-function relationships, while high-resolution evidence from crystallography is scarce. To explore the spectrum of substrate selectivity determinants in such families, it is important to introduce effective mutagenesis designs for the comprehensive *ab initio* study of new homologs, based on existing evidence from known members. Capitalization on data from Cys-scanning or other systematic analyses of a well-studied homolog, if available, offers a powerful approach to this end.

The above considerations apply promptly to the Nucleobase-Ascorbate Transporter (NAT)[1] or Nucleobase-Cation Symporter-2 (NCS2) family, an interesting example of a conserved but

Copyright 2012 by The American Society for Biochemistry and Molecular Biology, Inc.

Downloaded from www.jbc.org at UNIVERSITY OF IOANNINA, on March 27, 2012

functionally diverse group of transporters present in all major taxa of organisms. NAT transporters model on the template of the uracil permease UraA, the first and only x-ray structure to be described recently for a member of this family, which represents a novel fold (1). With respect to function, only 15 of more than 2,000 predicted members have been characterized in detail; these are specific for the cellular uptake of uracil, xanthine or uric acid (microbial, plant and non-primate mammalian genomes) or vitamin C (mammalian genomes) (1-3). Two of them, the xanthine permease XanQ of *Escherichia coli* (4-10) and the uric acid/xanthine permease UapA of *Aspergillus nidulans* (11-15) have been studied extensively with Cys-scanning mutagenesis and reverse and forward genetics, respectively. These studies have shown striking similarities between key NAT determinants of the two transporters, reinforcing the idea that few residues at conserved motifs of the family may be invariably critical for function or underlie specificity differences (for a summary of current knowledge, see supplemental Fig. S1). Based on homology modeling, most of these residues are found at the vicinity or at the periphery of the binding site in transmembrane segments TM1, TM3, TM8 and TM10 (1, 10, 15).

In the current work, we enrich the data set of functionally known NAT members by studying previously uncharacterized homologs from the genome of *E. coli* K-12 and we analyze function, substrate selectivity and the role of key residues in one of them (YgfU), using mutagenesis designs that are based on the well-studied homolog XanQ. Strikingly, the genome of *E. coli* K-12 contains 10 predicted members, of which functionally known are the uracil permease UraA (16) and the xanthine permeases XanQ and XanP (4). Of the remaining members, three cluster together with UraA, XanQ and XanP in COG2233 (YgfU, RutG, YbbY) and four cluster separately, in COG2252 (YgfQ, YjcD, YicO, PurP). Characteristic NAT sequence motifs are retained only by the three COG2233 members (Fig. 1*A*). Of them, RutG is related in sequence with the uracil permease UraA and is considered to be part of an unconventional pyrimidine utilization operon (17-19), while YgfU is found along with XanQ in a cluster of putative purine catabolic genes (20) and is related in sequence with xanthine or uric acid permeases from Gram-positive bacteria (21) (supplemental Table S1). The COG2252 members are more related in sequence with the fungal and plant AzgA-like adenine-guanine-hypoxanthine transporters (22, 23) and one of them (PurP) has been proposed to be a high-affinity adenine transporter, based on genetic (24) and systems biology evidence (25).

In the context of this work, we cloned and over-expressed YgfU and showed that it is a proton-gradient dependent, low-affinity (K_m 0.5 mM) and high-capacity transporter for uric acid which also transports xanthine, but with disproportionately low capacity. Subsequently, we subjected YgfU to site-directed mutagenesis, based on data available for the homologous xanthine permease XanQ, and found that residues irreplaceable for the mechanism occur at 5 highly conserved positions while a single-amino acid replacement (T100A) converts the uric acid-selective YgfU to a dual-selectivity transporter for both uric acid and xanthine. These results are supported with mirror-image replacements made in XanQ and homology modeling on the recently described structure of UraA.

Experimental Procedures

Materials – [8-^{14}C]uric acid (51.5 mCi mmol^{-1}), [8-^{3}H]xanthine (28 Ci mmol^{-1}) and [5,6-^{3}H]uracil (59 Ci mmol^{-1}) were purchased from Moravek Biochemicals. Non-radioactive nucleobases were from Sigma. Oligodeoxynucleotides were synthesized from BioSpring GmbH. High fidelity *Taq* Polymerase (Phusion High Fidelity PCR System) was from Finnzymes. Restriction endonucleases used were from Takara. Horseradish peroxidase (HRP)-conjugated avidin was from Amersham Pharmacia Biotech. All other materials were reagent grade and obtained from commercial sources.

Bacterial strains and plasmids – *E. coli* K-12 was transformed according to Inoue (26). TOP10F′ (Invitrogen) was used for initial propagation of recombinant plasmids. T184 (27) harboring pT7-5/*xanQ* or pT7-5/*ygfU* with given replacements was used for IPTG-inducible expression from the *lacZ* promoter/operator.

DNA manipulations – Construction of expression plasmids and BAD (biotin-acceptor domain)-tagged versions of NAT homologs was essentially as described previously for XanQ and XanP (4).

Downloaded from www.jbc.org at UNIVERSITY OF IOANNINA, on March 27, 2012

Briefly, the coding sequences of NAT genes were amplified by PCR on the template of genomic DNA prepared from *E. coli* T184 and transferred to plasmid vector pT7-5 by restriction fragment replacement; BAD-tagged versions were prepared using two-stage (overlap-extension) PCR (28) on the templates of pT7-5/*ygfU (or other NAT)* and pT7-5/*xanQ-BAD*. For construction of mutants, two-stage PCR was performed on the template of YgfU-BAD or XanQ-BAD, as indicated. The entire coding sequence of all engineered constructs was verified by double-strand DNA sequencing in an automated DNA sequencer (MWG-Biotech) (supplemental Table S2).

Growth of bacteria – *E. coli* T184 harboring given plasmids was grown aerobically at 37˚ C in Luria-Bertani medium containing streptomycin (0.01 mg/mL) and ampicillin (0.1 mg/mL). Fully grown cultures were diluted 10-fold, allowed to grow to mid-logarithmic phase, induced with IPTG (0.5 mM) for an additional 2 h at 37˚ C, harvested and washed with appropriate buffers.

Transport assays and kinetic analysis – *E. coli* T184 were assayed for active transport of [^{3}H]xanthine (0.1–250 μM), [^{3}H]uracil (1–100 μM) and [^{14}C]uric acid (0.01–2 mM), by rapid filtration, at 25˚ C and 37˚ C, pH 7.5, as described (4). For kinetic uptake measurements, initial rates were assayed in T184 cells, at 5-20 sec, and data were fitted to the Michaelis-Menten equation using *Prism*4, to determine K_m and V_{max} values. For ligand competition experiments with XanQ mutants, uptake of [^{3}H]xanthine (1 μM) was assayed in the absence or presence of unlabeled analogues (1 mM) (4-6).

Immunoblot analysis – Membrane fractions were prepared from 10 mL cultures of *E. coli* T184 harboring given plasmids and subjected to SDS-PAGE (12%), as described (4). Proteins were electroblotted to poly(vinylidene difluoride) membranes (Immobilon-PVDF; Pall Corp.). The BAD-tagged permeases were probed with avidin-HRP. Signals were developed with enhanced chemiluminescence (ECL).

In silico analysis – Comparative sequence analysis of NAT/NCS2 homologs was based on BLAST-p search and ClustalW alignment; the most recent genome annotations were used for retrieving sequence data. Initial analysis of transmembrane topology of YgfU was performed using program TMHMM (29). Homology threading was performed using the known x-ray structure of UraA as a template (PDB code 3QE7) on the web-based SWISSPROT modeling server (30); results were displayed and analyzed with PyMOL v1.4 (Schrödinger, LLC).

RESULTS

YgfU is a uric acid transporter – The NAT genes *ygfU*, *rutG*, *ybbY*, *ygfQ*, *yjcD*, *yicO* and *purP* were mobilized from the *E. coli* K-12 genome, transferred to transcriptional control of the *lacZ* promoter/operator in plasmid vector pT7-5 and induced for over-expression in *E. coli* T184 at conditions of negligible endogenous activity of oxidized purine or uracil uptake (4). Our data show that, with one exception, all NAT constructs can be expressed in the *E. coli* membrane at high levels, comparable to the ones of XanQ used as a control (Fig. 1*B*), while transport activity at 25˚ C is observed only with YgfU, which transports [^{14}C]uric acid (1 mM) to high levels, and RutG, which has a marginally detectable activity for [^{3}H]xanthine (1 μM) (Fig. 1*C*). Kinetic analysis reveals that RutG transports xanthine with 50-fold lower affinity (K_m 0.15 mM) in comparison with XanQ or XanP (4), and YgfU transports uric acid with low affinity (K_m 0.5 mM) and high capacity (V_{max} 715 nmol min^{-1} mg^{-1}) (Table 1). The steady-state level of uric acid accumulation achieved with YgfU after 2-15 min exposure to uric acid (1 mM) (Fig. 1*C*) is 381±4 nmol mg^{-1}; taking into account an internal volume for *E. coli* of about 5.8 μL mg^{-1} (31), this level corresponds to a concentration gradient of 128-fold (in/out). In addition, this uptake activity is abolished in the presence of the protonophore carbonyl cyanide-m-chlorophenyl hydrazone (CCCP) implying that transport is dependent on proton symport (32). With respect to xanthine uptake, YgfU displays a marginal xanthine uptake activity at 25˚ C, which precludes kinetic analysis, but it can transport xanthine at 37˚ C, albeit with very low affinity (K_m 0.3 mM; 100-fold higher than the K_m values of XanP or XanQ) and capacity (V_{max} 14 nmol min^{-1} mg^{-1}) (Table 1).

Delineation of mutagenesis targets for structure-function analysis of YgfU – The Cys-scanning and site-directed analysis of the homologous XanQ (5-10) offers a basis to search for targets of efficient mutagenesis designs in YgfU. Important residues

Downloaded from www.jbc.org at UNIVERSITY OF IOANNINA, on March 27, 2012

of XanQ have been delineated at positions where a side chain is irreplaceable with respect to function (Glu-272, Asp-304, Gln-324, Asn-325) or expression in the membrane (Gly-83, Pro-318), replaceable with a limited number of other side chains (His-31, Asn-93, Phe-94, Asp-276, Ala-279, Thr-280, Gly-305, Gly-351, Pro-354, Ile-432), or highly sensitive to inactivation of a substituted Cys mutant by *N*-ethylmaleimide (Leu-86, Val-261, Gly-275, Ser-284, Ala-323, Asn-326, Gly-327, Val-328, Ile-329, Thr-332, Gly-333, Ser-336, Asn-430). Most of these 29 residues are highly conserved in NAT/NCS2 family (Fig. 2) and YgfU differs from XanQ at 9 of the 29 positions (supplemental Fig. S1). To examine whether these residues contribute to the different substrate preference of YgfU we engineered mutants replacing each one of the 9 residues with the corresponding amino acid found in XanQ. Mutagenesis was also performed at conserved side chains corresponding to the four functionally irreplaceable residues of XanQ and His-31 which is essential for substrate affinity (7). Thus, our initial mutagenesis targets included His-37, Thr-100, Thr-259, Glu-270, Met-274, Leu-278, Val-282, Asp-298, Ser-317, Gln-318, Asn-319, Val-320, Arg-327, and Ser-426 (residues conserved in XanQ are underlined) (Fig. 3).

Site-directed mutagenesis of YgfU – Based on the above, we constructed and analyzed single-replacement mutants (a) E270D, E270N, E270Q, D298E, D298N, Q318N, Q318E, N319Q, N319D (conservative replacements of residues which are invariant and functionally irreplaceable in XanQ), (b) H37N, H37K, H37L, T100N, T100S, T100A (replacements of side chains which correspond to affinity- or specificity-related residues in XanQ), (c) T259V, M274D, L278T, V282S, S317A, V320N, R327G, S426N (replacements of non-conserved residues of the important set with the corresponding amino acid found in XanQ). In addition, prompted by our initial data (see below), we engineered replacements at positions of TM8 which correspond to moderately NEM-sensitive mutants (S256Q and S271A). The complete set of YgfU residues subjected to mutagenesis and their counterparts in XanQ is given in supplemental Fig. S1. After verification of the sequence, each YgfU mutant was transferred and expressed in *E. coli* T184 and assayed for its expression levels in the membrane and its ability to catalyze active transport of uric acid and xanthine (Fig. 4). Of the 25 mutants, four are undetectable in the membrane (T100N, S271A, M274D, V282S). Of the remaining 21 mutants, which display high protein levels comparable with wild type, 9 show negligible uptake activities for uric acid or xanthine (E270D, E270N, E270Q, D298E, N319Q, N319D, H37K, H37L, V320N). Of the 12 active mutants, four show marginal activity for uric acid uptake (5-12% of wild-type) (Q318N, Q318E, H37N, D298N), two accumulate uric acid at low (T100S, 20%) or intermediate levels (S317A, 40%) and six are highly active (60-120%) (T100A, S256Q, T259V, L278T, R327G, S426N). With respect to xanthine uptake, significant activities above the wild-type threshold are only attained by mutants T100A, T100S and S317A (Fig. 4*C*). Mutant T100A, in particular, which is highly active with both uric acid and xanthine, displays very significant xanthine uptake activity (about 50% of wild-type XanQ used as a control in these assays) even at 25˚ C, where wild-type YgfU is inactive (Fig. 5). Kinetic transport analysis shows that three mutants (T100S, R327G, S426N) have significantly lower affinity for uric acid than wild type (4-fold higher K_m values) while T100A does not differ significantly from wild type in affinity but displays a 10-fold higher V_{max} for uptake of xanthine at 37˚ C (Table 1). When comparing uric acid with xanthine uptake activity for wild-type and T100A, it is clear that this replacement converts the uric acid-selective YgfU to a dual-selectivity transporter for both uric acid and xanthine (Fig. 5*D*).

Mirror-image replacements in XanQ – In order to evaluate further the role of non-conserved YgfU residues, we performed reverse site-directed mutagenic analysis in XanQ. Each one of the 11 important residues of XanQ that differ in YgfU was replaced individually with the corresponding amino acid found in YgfU. Thus, we constructed XanQ mutants Q258S, V261T, A273S, T280L, S284V, A323S, N326V and N430S and assayed them for expression, uptake activity and substrate selectivity in parallel with mutants N93T (7), N93A (10), D276M (9) and G333R (8) that had been engineered by us in previous studies. As shown in Fig. 6, all these mutants are expressed in the *E. coli* membrane to high levels. Of them, two show negligible uptake activities for xanthine or

Downloaded from www.jbc.org at UNIVERSITY OF IOANNINA, on March 27, 2012

uric acid (Q258S, D276M), two display very low xanthine uptake activities (10-20% of wild-type) (N93T, N430S), 7 display intermediate xanthine uptake activities (40-60% of wild-type) (N93A, V261T, T280L, S284V, A323S, N326V, G333R), and one is highly active for xanthine uptake (100-120%) (A273S). On the other hand, only N93A shows a low but detectable uptake activity for uric acid (Fig. 6*C*). Kinetic transport analysis shows that five mutants have significantly lower affinity for xanthine than wild type (3-fold higher K_m values for mutants N93T, A323S, N326V, N430S and 6-fold higher K_m value for A273S) (Table 1). Finally, the specificity profile of each mutant was investigated by assaying the extent of inhibition of [^{3}H]xanthine uptake in the presence or absence of a series of purine analogues (Table 2). It is very interesting that, despite their inefficiency for uric acid uptake, most of these mutants allow the recognition of uric acid or other analogues that differ from xanthine at the imidazole moiety and are not recognized by wild type XanQ. Thus, uric acid inhibits N93A, V261T or G333R by 40-50%, 8-methylxanthine inhibits N93A or G333R by 80-90% and V261T, A273S, T280L, A323S or N326V by 50-70%, and 7-methylxanthine inhibits G333R by 80% (Table 2).

DISCUSSION

The results in this study yield important new knowledge in two respects. First, it is shown for the first time that the *E. coli* K-12 genome encodes a uric acid permease activity (YgfU). Second, key determinants of the substrate binding site function and specificity of this permease are delineated and Thr-100 in TM3 is demonstrated to be essential for the selectivity for uric acid.

The finding that the *ygfU* gene product in *E. coli* is a high-capacity transporter for uric acid raises questions on the putative physiological significance of such an uptake activity, since *E. coli* is not currently known to contain enzymes for uric acid catabolism or have a complete catabolic pathway for purines. Previous studies have shown that *E. coli* K-12 is unable to use purines other than adenine as sole nitrogen sources and, even with adenine, nitrogen assimilation is incomplete (20) but it can grow on allantoin as a sole nitrogen source, albeit only at anaerobic conditions (33). It also contains xanthine dehydrogenase activity (20) which can divert hypoxanthine and xanthine from the purine salvage pathway and produce uric acid. The missing link, however, is in the catabolic oxidation of uric acid to allantoin.

As shown relatively recently (34), the oxidation of uric acid to allantoin is expected to involve three enzymatic steps, the first one catalyzed by urate oxidase and yielding 5-hydroxy-isourate (HIU), the second one catalyzed by HIU hydrolase which converts HIU to 2-oxo-4-hydroxy-4-carboxy-5-ureidoimidazoline (OHCU) and the third one catalyzed by OHCU decarboxylase which converts OHCU to dextrorotatory S-(+)-allantoin, the substrate for (S)-allantoin amidohydrolase (AllB) (35). In *E. coli* K-12, no enzymatic activity or any candidate *E. coli* gene has been reported for the step of oxidation of uric acid to HIU, while HIU hydrolase (HiuH) and, suggestively, OHCU decarboxylase activity has been assigned experimentally to the product of gene *yedX* (EcoGene database, and Kenneth Rudd, personal communication). Interestingly, *E. coli* HiuH and its *Bacillus subtilis* homolog PucM (36) show clear sequence and structural similarity with the vertebral thyroid hormone distributor protein transthyretin, which probably originated from a duplication of an ancestral HIU hydrolase gene (37). In contrast to most bacterial homologs, the HiuH genes from *E. coli* and other enterobacteria appear not to be associated with purine metabolism operons and have been suggested to encode proteins with periplasmic localization which might utilize HIU produced by a spontaneous, non-enzymatic reaction of uric acid acting as an antioxidant in the periplasm (38).

On the other hand, a complete gene cluster for purine utilization (*hpx* cluster) has been recently identified in *Klebsiella pneumoniae* (39) and *Klebsiella oxytoca* (40) containing separate genes for all three enzymatic steps of uric acid oxidation, namely *hpxO* (urate hydroxylase), *hpxT* (HIU hydrolase) and *hpxQ* (OHCU decarboxylase). Apart from HpxT (HiuH), which is homologous to *E. coli* HiuH and *B. subtilis* PucM, HpxO was found to function as a novel FAD-dependent urate oxidase (41), distinct from the classical urate oxidase (uricase) known for *B. subtilis* (36) and other species with complete purine utilization pathways (42). Parts of the *hpx* gene cluster of *Klebsiella* including the HpxO

Downloaded from www.jbc.org at UNIVERSITY OF IOANNINA, on March 27, 2012

homolog are also encountered in other gamma-proteobacterial genera like *Xanthomonas* and *Acinetobacter* (40) but not in *E. coli*. Finally, the *hpx* cluster contains a single putative permease gene (*hpxP*) which was suggested to encode a general purine permease (40). HpxP belongs to the NAT/NCS2 family and is closely homologous with the *E. coli* xanthine permease XanQ (45% sequence identity) but shares limited sequence homology with YgfU (25% identity).

Overall, it appears that there is more to learn on the purine utilization pathways in *E. coli* K-12 and our identification of YgfU as a uric acid transporter is an important contribution to this end. Although YgfU is found along with XanQ in a cluster of putative purine catabolic genes (20), this cluster does not appear to contain homologs for catabolic utilization of uric acid. In addition, YgfU has a limited array of orthologs in gamma-proteobacteria (for example, only six homologs with >50% identity in other enterobacteria) but it shares up to 50% sequence identity with many homologs from Gram-positive bacteria including the known xanthine permease PbuX and uric acid permeases PucJ and PucK from *B. subtilis* (supplemental Table S1). Apart from uric acid, YgfU can utilize as a substrate xanthine, but with disproportionately low capacity which is only apparent at 37˚ C (Fig. 5 and Table 1). In addition, the affinity of YgfU for xanthine is very low relative to the ones of the xanthine permeases XanP and XanQ (4). Based on the above, the major substrate transported by YgfU appears to be uric acid and we would like to suggest UacT (uric acid transporter) as an alternative, function-based designation for YgfU.

The comprehensive mutagenesis study of YgfU (UacT) presented herein reveals the key role of His-37 (TM1), Glu-270 (TM8), Asp-298 (TM9), Gln-318 and Asn-319 (TM10), which are functionally irreplaceable, and of Thr-100 (TM3), which is essential for the uric acid selectivity. Structural modeling of YgfU based on the known x-ray structure of the uracil-transporting homolog UraA (1) shows that five of the six important residues fall at transmembrane helices which form a binding shelter around substrate and at least three of them (Glu-270, Gln-318, Thr-100) are in the substrate binding pocket (Fig. 7). In other members of the NAT/NCS2 family, these residues are either absolutely conserved (His-37, Glu-270, Asn-319) or conform to a distinct conservation pattern with limited side chain changes (Fig. 2). Most importantly, as well, critical roles have been described for the corresponding residues of other known NAT homologs (1, 7-13, 43), as addressed in more detail below.

The five irreplaceable YgfU residues are conserved in the xanthine-transporting homolog XanQ and the dual-specificity uric acid/xanthine transporter UapA and four out of five are also irreplaceable for function in XanQ (8, 9) and in UapA (12, 13). The irreplaceable role of the counterparts of Gln-318 and Asn-319, which belong to the conserved nucleobase-ascorbate transporter (NAT) signature motif (11), has been linked with defining the function of the binding site in both XanQ (5, 8) and UapA (12, 13), and site-directed alkylation studies in XanQ have implied that the corresponding residues interact directly with purine substrate (8). In the known x-ray structure of the pyrimidine-specific homolog UraA (1), the position of Gln-318 is occupied by a Glu (Glu-290) which forms two direct hydrogen bonds with substrate (uracil); the counterpart of Asn-319 (Asn-291) stabilizes the structure through an indirect hydrogen bonding effect involving the counterpart of His-37 (His-24) in TM1. The role of another irreplaceable YgfU residue (Glu-270) might also be linked directly with binding, since its counterpart in UraA (Glu-241) also forms two direct hydrogen bonds with substrate in the crystal structure (1). The fourth invariably irreplaceable residue (Asp-298 in YgfU) corresponds to a position of UraA which is at the same depth in the membrane but distal from the binding site in the crystal structure and might have a distinct conformational role in the purine translocation mechanism, as suggested for permease XanQ (7, 9). In any event, the fact that four conserved residues associated either directly or indirectly with binding are functionally irreplaceable in both XanQ, YgfU (UacT) and UapA highlights the functional conservation of the purine binding site in NAT/NCS2 homologs of different selectivity.

His-37 (TM1) is absolutely conserved in the NAT/NCS2 family. Although replaceable in transporters other than YgfU, this histidine appears to be irreplaceable for function in YgfU (Fig. 4). From the other homologs, which include the bacterial XanQ (7), the fungal UapA (15) and

Downloaded from www.jbc.org at UNIVERSITY OF IOANNINA, on March 27, 2012

the mammalian hSVCT1 (43) and hSVCT2 (44), a conserved hydrogen bonding role is apparent for this residue, which is crucial for either the overall structural folding or the constitution of a proper affinity and specificity binding site or for both. Namely, presence of an uncharged hydrogen-bonding residue at this position is essential for high affinity binding and transport in XanQ (7) and in the hSVCTs (43, 44), while in UapA it has been suggested as crucial for proper folding and targeting to the plasma membrane (15). The recently elucidated crystal structure of the different-specificity homolog UraA (1) as well as homology models built on this structure (10, 15) show that the conserved His of TM1 hydrogen bonds to the conserved Asn of the NAT signature motif at the binding site periphery, substantiating further the previous findings. Based on the mutagenesis data of Fig. 4, it appears that this hydrogen bonding interaction between His-37 and Asn-319 (Fig. 7) is more stringent in YgfU than in other homologs and it may play an irreplaceable role with respect to the binding site integrity in this transporter.

Replacement of Thr-100 (TM3) with Ala changes the uric acid-selective YgfU to a dual-selectivity variant transporting both uric acid and xanthine with comparable efficiencies (Fig. 5) and replacement of the same residue with Ser also allows improved xanthine uptake relative to the uric acid uptake activity (Fig. 4). Thus, the side chain of Thr-100 is linked with the transporter ability to differentiate between uric acid (8-oxy-xanthine) and xanthine. A similar role has been proposed for the corresponding amino acid in permease XanQ (Asn-93) since replacement of Asn-93 with Ala or Ser converts the xanthine-selective XanQ to dual-selectivity variants (7, 10); in the case of XanQ, however, the dual-selectivity variants transport the non-wild type substrate (uric acid) with very low capacity (10). The selectivity-related role of Thr-100/Asn-93 appears to be unique, since no other single-replacement mutant of either XanQ (6-10) or YgfU (this study) has been shown to convert the native transporter to a dual-selectivity one. Interestingly, a similar albeit less prominent effect was observed with mutants replacing the corresponding residue (Ser-154) in the fungal homolog UapA, where introduction of an Ala leads to higher affinity for xanthine relative to uric acid thus shifting the dual-selectivity profile to the xanthine-selective direction (15).

Although the side chains of Thr-100 or Asn-93 per se are poorly conserved in other homologs (10), the polar character of Thr-100/Asn-93 is conserved invariably in the known nucleobase-transporting NAT members (Asn, Thr or Ser) while the ascorbate-transporting members have an Ala (Fig. 2). Furthermore, all the dual-selectivity uric-acid/xanthine transporters (Xut1, UapA, UapC, AfUapA, Lpe1) have a Ser at this position (Fig. 2). To understand the structural relevance of this difference, we have built models of the xanthine-selective XanQ, the uric acid-selective YgfU and the dual-selectivity fungal homologs on the template of the known structure of UraA (Fig. 7 and data not shown). The models indicate that the relevant position of TM3 is vicinal to the substrate binding site formed between residues of the middle parts of TM3, TM8 and TM10 (1). Strikingly, however, the Thr or Ser replacing Asn-93 in YgfU and all dual-selectivity NATs is distal from the conserved, substrate-relevant glutamate of TM8 (minimal distance between oxygen atoms, 6.0 Å) while Asn-93 in XanQ is significantly closer (distance between oxygen atoms, 4.5 Å). This difference is most prominent in YgfU (Fig. 7) and UapA (10) which conserve nearly all the other functionally important residues of TM1, TM3, TM8 or TM10, except Asn-93.

In UapA (10, 15), occupation of the Asn-93 position by Ser orients this residue away from the substrate-relevant Glu of TM8, leading to relaxation of a constraint for the recognition of analogues at position 8 and allowing binding and transport of uric acid (8-oxy-xanthine), which shifts the NAT selectivity to a less stringent, dual-substrate profile. Accordingly, the XanQ mutants replacing Asn-93 with Ser or Ala yield efficient recognition of 8-methylxanthine and low but significant uptake of uric acid, mimicking in part the fungal, dual-selectivity NATs (10).

In YgfU, Thr-100 is also oriented away from the carboxyl group of Glu-270 (TM8) leaving more space in the substrate binding pocket but, at the same time, the pKa of Glu-270 may be distorted significantly relative to the corresponding carboxylic acid in XanQ due to its vicinity with hydrophobic groups from Thr-100 and Met-274 (Fig. 7*B*). These changes on the

Downloaded from www.jbc.org at UNIVERSITY OF IOANNINA, on March 27, 2012

substrate binding Glu-272/Glu-270 might account for the selectivity difference between YgfU (uric acid) and XanQ (xanthine). Interestingly, however, replacement of Asn-93 with Thr in XanQ cannot imitate the YgfU profile but leads to low affinity for all xanthine analogues, possibly due to interference of the methyl group of Thr-93 in the vicinity of the essential Glu-272 which is not counterbalanced by other changes (10). An even more dramatic effect is observed in the current study with the mirror-image YgfU replacement T100N which leads to complete lack of expression in the membrane (Fig. 4). Based on these observations, it is evident that further combinatorial replacements are needed to promptly convert XanQ to the YgfU selectivity profile or vice versa and targets for such replacements can be selected from residues of the important set analyzed here (Fig. 2) taking into account their orientation relative to the binding site in the modeled structures and functional properties of the relevant single-replacement mutants.[2]

Apart from the results discussed above, our initial mutagenic analysis of YgfU permease revealed that site-specific replacements at TM8 (S271A, M274D, V282S) impair expression in the membrane, V320N (TM10) inactivates, S317A (TM10) allows substantial uptake of xanthine, and R327G (TM10) or S426N (TM14) reduces the affinity for uric acid (four-fold increased K_m). The significance of these additional findings will be evaluated further with ongoing mutagenesis studies in this and other NAT homologs.[3] In any event, it is important to note that several mutants of YgfU at positions of TM8, TM10, TM3 and TM1 flanking the binding site in the modeled structure lead to grossly impaired activity (H37N, V320N) or lack of expression in the membrane (T100N, S271A, M274D, V282S) while their counterpart or mirror-image replacement mutants in XanQ are active and expressed normally (Fig. 6). This observation implies that the binding site of YgfU is more prone to destabilization induced by peripheral side chain changes, while the reciprocal changes in XanQ are permissive for structure and function.

Finally, from a methodological point of view, it should be emphasized that all the results presented here for YgfU permease were based on site-directed mutagenesis designs deduced from Cys-scanning analysis data of a well-studied homolog (XanQ). In this respect, we have shown that comprehensive analysis of structure-function relationships in a newly characterized transporter can be accomplished with relatively few site-directed replacements, based on the knowledge available from Cys-scanning mutagenesis of a prototypic homolog.

Downloaded from www.jbc.org at UNIVERSITY OF IOANNINA, on March 27, 2012

REFERENCES

1. Lu, F., Li, S., Jiang, Y., Jiang, J., Fan, H., Lu, G., Deng, D., Dang, S., Zhang, X., Wang, J., and Yan, N. (2011) *Nature* **472**, 243-246.
2. Yamamoto, S., Inoue, K., Murata, T., Kamigaso, S., Yasujima, T., Maeda J., Yoshida, Y., Ohta, K., and Yuasa, H. (2010). *J. Biol. Chem.* **285**, 6522-6531.
3. Tsukaguchi, H., Tokui, T., Mackenzie, B., Berger, U. V., Chen, X. Z., Wang, Y., Brubaker, R. F., and Hediger, M. A. (1999). *Nature* **399**, 70-75.
4. Karatza, P., and Frillingos, S. (2005). *Mol. Membr. Biol.* **22**, 251-261.
5. Karatza, P., Panos, P., Georgopoulou, E., and Frillingos, S. (2006). *J. Biol. Chem.* **281**, 39881-39890.
6. Papakostas, K., Georgopoulou, E., and Frillingos, S. (2008). *J. Biol. Chem.* **283**, 13666-13678.
7. Karena, E., and Frillingos, S. (2009). *J. Biol. Chem.* **284**, 24257-24268.
8. Georgopoulou, E., Mermelekas, G., Karena, E., and Frillingos, S. (2010). *J. Biol. Chem.* **285**, 19422-19433.
9. Mermelekas, G., Georgopoulou, E., Kallis, A., Botou M., Vlantos, V., and Frillingos, S. (2010). *J. Biol. Chem.* **285**, 35011-35020.
10. Karena, E., and Frillingos, S. (2011). *J. Biol. Chem.* **286**, 39595-39605.
11. Diallinas, G., Valdez, J., Sophianopoulou, V., Rosa, A., and Scazzocchio, C. (1998). *EMBO J.* **17**, 3827-3837.

12. Koukaki, M., Vlanti, A., Goudela, S., Pantazopoulou, A., Gioule, H., Tournaviti, S., and Diallinas, G. (2005). *J. Mol. Biol.* **350**, 499-513.
13. Papageorgiou, I., Gournas, C., Vlanti, A., Amillis, S., Pantazopoulou, A., and Diallinas, G. (2008). *J. Mol. Biol.* **382**, 1121-1135.
14. Kosti, V., Papageorgiou, I., and Diallinas, G. (2010). *J. Mol. Biol.* **397**, 1132-1143.
15. Amillis, S., Kosti, V., Pantazopoulou, A., Mikros, E., and Diallinas, G. (2011). *J. Mol. Biol.* **411**, 567-580.
16. Andersen, P.S., Frees, D., Fast R., and Mygind, B. (1995). *J. Bacteriol.* **177**, 2008-2013.
17. Loh, K. D., Gyaneshwar, P., Markenscoff-Papadimitriou, E., Fong, R., Kim, K.-S., Parales, R., Zhou, Z., Inwood, W., and Kustu, S. (2006). *Proc. Natl. Acad. Sci. USA* **103**, 5114-5119.
18. Kim, K. S., Pelton, J.G., Inwood, W. B., Andersen, U., Kustu, S., and Wemmer, D. E. (2010). *J. Bacteriol.* **192**, 4089-4102.
19. Parales, R. E., and Ingraham, J. L. (2010). *J. Bacteriol.* **192**, 4086-4088.
20. Xi, H., Schneider, B. L., and Reitzer, L. (2000). *J. Bacteriol.***182**, 5332-5341.
21. Schultz, A. C., Nygaard, P., and Saxild, H. H. (2001). *J. Bacteriol.* **183**, 3293-3302.
22. Cecchetto, G., Amillis, S., Diallinas, G., Scazzocchio, C., and Drevet, C. (2004). *J. Biol. Chem.* **279**, 3132-3141.
23. Mansfield, T. A., Schultes, N. P., and Mourad, G. S. (2009). *FEBS Lett* **583**, 481-486.
24. Burton, K. (1994). *Proc Biol Sci* **255**, 153-157.
25. Cho, B. K., Federowicz, S. A., Embree, M., Park, Y. S., Kim, D., and Palsson, B. Ø. (2010). *Nucleic Acids Res* **39**, 6456-6464.
26. Inoue, H., Nojima, H., and Okayama, H. (1990). *Gene* **96**, 23-28.
27. Teather, R. M., Bramhill, J., Riede, I., Wright, J. K., Furst, M., Aichele, G., Wilhelm, V., and Overath, P. (1980). *Eur. J. Biochem.* **108**, 223-231.
28. Ho, S. N., Hunt, H. D., Horton, R. M., Pullen, J. K., and Pease, L. R. (1989). *Gene* **77**, 51-59.
29. Granseth, E., Daley, D. O., Rapp, M., Melen, K., and von Heijne, G. (2005). *J. Mol. Biol.* **352**, 489-494.
30. Schwede, T., Kopp, J., Guex, N., and Peitsch, M. C. (2003). *Nucleic Acids Res.* **31**, 3381-3385.
31. Felle, H., Porter, J. S., Slayman, C. L., and Kaback, H. R. (1980). *Biochemistry* **19**, 3585-3590.
32. Kaback, H. R., Reeves, J. P., Short, S. A., and Lombardi, F. J. (1974). *Arch. Biochem. Biophys.* **160**, 215-222.
33. Cusa, E., Obradors, N., Baldoma, L., Badia, J., and Aguilar, J. (1999). *J. Bacteriol.***181**, 7479-7484.
34. Ramazzina, I., Folli, C., Secchi, A., Berni, R., and Percudani, R. (2006). *Nature Chem. Biol.* **2**, 144-148.
35. Rintoul, M. R., Cusa, E., Baldoma, L., Badia, J., Reitzer, L., and Aguilar, J. (2002). *J. Mol. Biol.***324**, 599-610.
36. Lee, Y., Lee, D. H., Kho, C. W., Lee, A. Y., Jang, M., Cho, S., Lee, C. H., Lee, J. S., Myung, P. K., Park, B. C., and Park, S. G. (2005). *FEBS Lett.* **579**, 4769-4774.
37. Zanotti, G., Cendron, L., Ramazzina, I., Folli, C., Perducani, R., and Berni, R. (2006). *J. Mol. Biol.* **363**, 1-9.
38. Hennebry, S. C. (2009). *FEBS J.* **276**, 5367-5379.
39. de la Riva, L., Badia, J., Aguilar, J., Bender, R. A., and Baldoma, L. (2008). *J. Bacteriol.***190**, 7892-7903.
40. Pope, S. D., Chen, L.-L., and Stewart, V. (2009). *J. Bacteriol.***191**, 1006-1017.
41. O'Leary, S. E., Hicks, K. A., Ealick, S. E., and Begley, T. P. (2009). *Biochemistry* **48**, 3033-3035.
42. Gournas, C., Oestreicher, N., Amillis, A., Diallinas, G., and Scazzocchio, C. (2011). *Fungal Genet. Biol.* **48**, 840-848.
43. Ormazabal, V., Zuñiga, F. A., Escobar, E., Aylwin, C., Salas-Burgos, A., Godoy, A., Reyes, A. M., Vera, J. C., and Rivas, C. I. (2010). *J. Biol. Chem.* **285**, 36471-36485.
44. Varma, S., Campbell, C., and Kuo, S. (2008). *Biochemistry* **47**, 2952-2960.

Downloaded from www.jbc.org at UNIVERSITY OF IOANNINA, on March 27, 2012

FOOTNOTES

*This paper is part of the research project EVOTRANS co-funded by the European Union – European Social Fund (ESF) and National Sources, in the framework of program "Thalis" through the Operational Program "Education and Lifelong Learning" of the Hellenic Ministry of Education, Lifelong Learning and Religious Affairs, in the context of the National Strategic Reference Framework (NSRF). We thank Dr. Kenneth Rudd for helpful discussions on an appropriate function-based designation for YgfU.

[1]The abbreviations used are: NAT, nucleobase-ascorbate transporter; TM, transmembrane segment; NEM, *N*-ethylmaleimide; HRP, horseradish peroxidase; IPTG, isopropyl 1-thio-β,D-galactopyranoside; BAD, biotin-acceptor domain; CCCP, cyanide-m-chlorophenyl hydrazone.

[2]Ekaterini Karena, Konstantinos Papakostas, and Stathis Frillingos, in preparation

[3]Maria Botou, Konstantinos Papakostas, and Stathis Frillingos, in preparation

FIGURE LEGENDS

Fig. 1. **Sequence, immunoblot and nucleobase uptake analysis of NAT homologs from *E. coli***. The full-length sequences of NAT members from *E. coli* K-12 were aligned using ClustalW and part of this alignment referring to conserved sequence motifs of the family is shown in ***A***. The members include the known nucleobase transporters XanQ (P67444), XanP (P0AGM9) and UraA (P0AGM7) and the unknown YgfU (Q46821), RutG (P75892), YbbY (P77328), YgfQ (Q46817), YjcD (P0AF52), YicO (P31440) and PurP (P31466). The motifs shown are characteristic for functionally known members of the family and have been shown to contain functionally important residues in XanQ (6-10). Sequence identity scores are shown on the right. The coding sequences from the unknown homologs were mobilized from the genome, induced for over-expression in *E. coli* T184 under control of the *lacZ* promoter/operator in pT7-5/*NAT*-BAD and assayed for expression levels in the membrane and active transport of xanthine, uracil and uric acid. Samples containing 100 μg of membrane protein were subjected to SDS-PAGE (12%) and immunoblotting using HRP-conjugated avidin (***B***). Cells expressing each homolog were normalized to 0.7 mg protein per mL of cell suspension and assayed for active transport of [^{14}C]uric acid (1 mM, 25° C) in the presence of absence of CCCP (10 μM) (***C***). Transport assays were also performed for [^{3}H]xanthine (1 μM, 25° C), using XanQ as a positive control (4), and for [^{3}H]uracil (1 μM, 25° C). Uracil uptake could not be detected with any of the unknown homologs; xanthine uptake was observed only with RutG, albeit to a marginal extent (not shown).

Fig. 2. **Conservation pattern of important residues of XanQ in NAT family**. A logotype of 29 residues delineated as important from the Cys-scanning analysis of XanQ (5-10) is shown on *top*. Larger-size letters indicate irreplaceable XanQ residues, medium size indicates residues that are replaceable with a limited number of side chains and smaller size indicates residues where a Cys replacement is highly sensitive to inactivation by NEM (IC_{50} < 100 μM). A perpendicular line indicates a residue where replacements distort specificity for the imidazole moiety of substrate (leading to aberrant recognition of uric acid and 8-methylxanthine). *Italics* indicate residues that are crucial (smaller size) or irreplaceable (larger size) for expression in the membrane. The histogram in the *upper panel* shows the number and relative abundance of different amino acids found at each position of the important set in the 189 closest homologs (> 33% sequence identity with XanQ) (10); the corresponding variants are listed in decreasing order of frequency while variants with very low occurrence (≤1.6%) are omitted for clarity. The sequence alignments in the *lower panel* show the residues found at each position of the important set in 15 characterized NAT/NCS2 transporters, including *Escherichia coli* XanQ (P67444), XanP (P0AGM9) and UraA (P0AGM7), *Bacillus subtilis* PbuX (P42086), PucK (O32140), and PucJ (O32139), *Lactococcus lactis* PyrP (AAK05701), *Aspergillus nidulans* UapA (Q07307) and UapC (P487777), *A. fumigatus* AfUapA (XP748919), *Candida albicans* Xut1 (AAX2221), *Zea mays* Lpe1 (AAB17501), *Homo sapiens*

Downloaded from www.jbc.org at UNIVERSITY OF IOANNINA, on March 27, 2012

SVCT1 (SLC23A1) (AAH50261) and SVCT2 (SLC23A2) (Q9UGH3) and *Rattus norvegicus* SNBT1 (SLC23A4) (AB511909). The full-length sequences were aligned using ClustalW and part of this alignment including the residues of interest is presented. Major substrates of each transporter are shown in parentheses on the left. The abbreviations are Xan (xanthine), UA (uric acid), Ura (uracil) and Asc (ascorbate).

Fig. 3. **Topology model of YgfU permease and mutagenesis targets**. The model is derived from homology threading using the UraA structure (3QE7) as a template and initial topology predictions based on program TMHMM and analysis of the XanQ homolog for the accessibility of loops to hydrophilic reagents (8). The α-helical segments are indicated in rectangles with continuous (core domain) or broken-line perimeters (gate domain). Residues corresponding to the ones analyzed with Cys-scanning mutagenesis in XanQ are *circled*. Residues corresponding to the important set (Fig. 2) are shown in *dark background* (functionally important in XanQ) or in a *bold circle* (crucial for expression in XanQ). Residues corresponding to positions of XanQ mutants that are moderately sensitive to NEM (IC_{50} values from 100 μM to 1 mM) are in *grey background*. The residues of YgfU analyzed in this study with site-directed mutagenesis are numbered and shown in *blue* (irreplaceable for function), *red* (essential for the counter-selectivity against xanthine), *dark red* (replacements lead to lower affinity for uric acid), *orange* (replacements lead to abolishment of expression in the membrane), or grey scale (remaining positions).

Fig. 4. **Expression and uptake activities of YgfU mutants**. *E. coli* T184 harboring pT7-5/*ygfU*(wild-type-BAD) with given mutations were grown aerobically to mid-logarithmic phase, induced with IPTG (0.5 mM) for 2 h, and subjected to immunoblot analysis of membrane fractions or assayed for transport of [^{14}C]uric acid (1 mM, 25° C) and [^{3}H]xanthine (0.1 mM, 37° C). ***A***, Samples containing approximately 100 μg of membrane protein were subjected to SDS-PAGE (12%) and immunoblotting using HRP-conjugated avidin. Prestained molecular mass standards (in kDa; Bio-Rad, low range) are shown on the left. ***B***, Initial rates of uric acid uptake (closed histogram bars) were measured at 5-15 sec and steady state levels of uric acid accumulation (open histogram bars) were measured at 2-10 min. Control values obtained from T184 harboring pT7-5 alone were subtracted from the sample measurements in all cases. Results are expressed as a percentage of the activity of wild-type control with standard deviations from three independent determinations. ***C***, Comparison of initial rates of uric acid and xanthine uptake for the active YgfU mutants. Results are expressed as a percentage of the rate of YgfU and XanQ, respectively. The percentage ratio of the xanthine uptake value (*red*) to the uric acid uptake value (*black*) is given for each mutant in a third histogram bar (*blue*).

Fig. 5. **Analysis of substrate selectivity for mutant T100A**. *E. coli* T184 harboring pT7-5/*ygfU*(wild-type-BAD), pT7-5/ *ygfU*(T100A-BAD), pT7-5/*xanQ*(wild-type-BAD) or pT7-5 alone were grown, induced and assayed for transport of [^{14}C]uric acid (0.01-2 mM, 25° C) and [^{3}H]xanthine (0.1 μM-0.25 mM, 37° C or 25° C), as described in the legend to Fig. 4 and Table 1. ***A***, Time courses of xanthine (0.1 mM) uptake at 37° C. ***B***, Time courses of xanthine (0.1 mM) uptake at 25° C. ***C***, Time courses of uric acid (1 mM) uptake at 25° C. ***D***, Comparison of the transport efficiencies (V_{max}/K_m) for uric acid (25° C) and xanthine (37° C) displayed by YgfU and T100A (see also Table 1). The abbreviations are UA (uric acid) and X (xanthine).

Fig. 6. **Expression and uptake activities of XanQ mutants.** *E. coli* T184 harboring pT7-5/*xanQ*(wild-type-BAD) with given mutations were grown, induced and subjected to immunoblot analysis of membrane fractions (***A***) or assayed for transport of [^{3}H]xanthine (1 μM, 25° C) (***B***) and [^{14}C]uric acid (2 mM, 25° C) (***C***), exactly as described in the legend to Fig. 4. Closed and open histogram bars represent initial rate and steady-state values, respectively.

Fig. 7. **Arrangement of important residues in the modeled structure of YgfU.** The sequences of YgfU and XanQ were threaded on the known x-ray structure of UraA (1) using the SWISSPROT modeling

Downloaded from www.jbc.org at UNIVERSITY OF IOANNINA, on March 27, 2012

server. The structural models were displayed with PyMOL v1.4. Shown are four TMs which contain binding residues and form a shelter around substrate in UraA, namely TM1 (*grey*), TM3 (*wheat*), TM8 (*teal*) and TM10 (*salmon*). ***A***, Arrangement of the four TMs in the YgfU model. ***B***, The same model (YgfU) excluding the β-strand regions of TM3 and TM10 and indicating the side chains of residues analyzed with mutagenesis in this study. ***C***, Arrangement of the corresponding residues and helices in XanQ. The side chains of important residues of YgfU (***B***) and XanQ (***C***) are shown as thick sticks (irreplaceable and/or substrate binding-relevant) or spheres (sensitive to alkylation or bulky replacement in XanQ; crucial for the protein expression or affinity in YgfU). The side chain of T100 (or N93) which is associated with the uric acid selectivity is shown with *red label*.

Downloaded from www.jbc.org at UNIVERSITY OF IOANNINA, on March 27, 2012

Table 1. K_m and V_{max} values of YgfU, XanQ and mutants

Permease	K_m (mM)	V_{max} (nmol min^{-1} mg^{-1} protein)	V_{max}/K_m (μL min^{-1} mg^{-1})
Kinetics for uric acid uptake (25˚ C)			
YgfU(wt)	0.5 ± 0.1	715 ± 81	1430
H37N	1.4 ± 0.3	23 ± 8	16
H37K/L	ND	ND	
T100A	0.9 ± 0.4	700 ± 160	777
T100S	1.9 ± 0.7	296 ± 87	159
S256Q	0.8 ± 0.1	698 ± 50	872
T259V	0.8 ± 0.3	808 ± 150	1049
L278T	0.6 ± 0.3	609 ± 165	1015
E270D/N/Q	ND	ND	
D298E/N	ND	ND	
S317A	0.5 ± 0.2	535 ± 104	1070
Q318N/E	ND	ND	
N319Q/D	ND	ND	
V320N	ND	ND	
R327G	2.2 ± 0.9	2064 ± 565	938
S426N	1.9 ± 0.3	808 ± 150	946
Kinetics for xanthine uptake (37˚ C and 25˚ C)			
Permease	K_m (μM)	V_{max} (nmol min^{-1} mg^{-1} protein)	V_{max}/K_m (μL min^{-1} mg^{-1})
YgfU(wt) (25˚ C)	ND	ND	
YgfU(wt) (37˚ C)	300 ± 60	14 ± 4	46
T100A (37˚ C)	240 ± 5	132 ± 20	550
T100S	ND	ND	
XanQ(wt) (25˚ C)	4.1 ± 0.5	7.2 ± 1.1	1756
N93T	11.6 ± 2.9	5.0 ± 0.4	431
N93A	2.4 ± 0.7	5.0 ± 0.5	2083
Q258S	ND	ND	
V261T	7.4 ± 0.7	23.2 ± 0.8	3135
A273S	24.1 ± 0.5	113.1 ± 3.5	4688
D276M	ND	ND	
T280L	4.3 ± 0.3	14.8 ± 0.4	3442
S284V	5.1 ± 0.5	8.8 ± 0.3	1725
A323S	13.9 ± 4.1	37.5 ± 4.5	2698
N326V	11.4 ± 1.4	23.1 ± 1.0	2026
G333R	2.8 ± 0.3	2.4 ± 0.2	857
N430S	12.0 ± 1.3	6.6 ± 0.3	550

E. coli T184 expressing the corresponding constructs were assayed for initial rates of [^{14}C]uric acid (0.01–2 mM) and [^{3}H]xanthine (0.1-250 μM) uptake at 5-20 sec, at either 25˚ C or 37˚ C, as given; negative

Downloaded from www.jbc.org at UNIVERSITY OF IOANNINA, on March 27, 2012

control values obtained from T184 harboring vector pT7-5 alone were subtracted from the sample measurements in all cases. Kinetic parameters were determined from non-linear regression fitting to the Michaelis-Menten equation using *Prism*4; values represent the means of three independent determinations with standard deviations shown. ND, assays were performed, but kinetic values were not determined due to very low uptake rates. All mutants and the wild-type versions used contained a carboxyl-terminal biotin-acceptor domain (BAD).

Downloaded from www.jbc.org at UNIVERSITY OF IOANNINA, on March 27, 2012

Table 2. Specificity profile of XanQ mutants

	Xanthine uptake rate retained (%)										
Xanthine analogue used as competitor	XanQ	N93T	N93A	V261T	A273S	T280L	S284V	A323S	G333R	N326V	N430S
Imidazole moiety											
Uric acid	96	115	**60**	**55**	102	102	98	100	**50**	100	75
8-methylxanthine	96	69	**10**	**48**	**39**	**37**	82	**33**	**18**	**35**	81
7-methylxanthine	105	121	62	69	75	74	92	61	**20**	63	69
Oxypurinol	31	13	2	39	17	8	16	14	10	44	45
Pyrimidine moiety											
2-thioxanthine	14	43	16	34	12	6	32	0	12	24	18
3-methylxanthine	25	49	41	55	50	18	29	6	1	42	29
6-thioxanthine	20	**84**	24	42	15	11	30	5	11	36	42

E. coli T184 expressing the corresponding constructs were assayed for initial rates of [^{3}H]xanthine (1 μM) uptake at 5-20 sec, in the absence or presence of 1000-fold excess (1 mM) of unlabeled competitors. The uptake value obtained in the absence of competitor was taken as 100%. Values represent the means of three determinations, with standard deviations <20%. Most significant differences from the wild-type profile are highlighted in bold. All mutants and the wild-type XanQ version used contained a carboxyl-terminal biotin-acceptor domain (BAD). Data on mutants N93T/A and G333R are from ref. 10 and ref. 8, respectively.

Downloaded from www.jbc.org at UNIVERSITY OF IOANNINA, on March 27, 2012

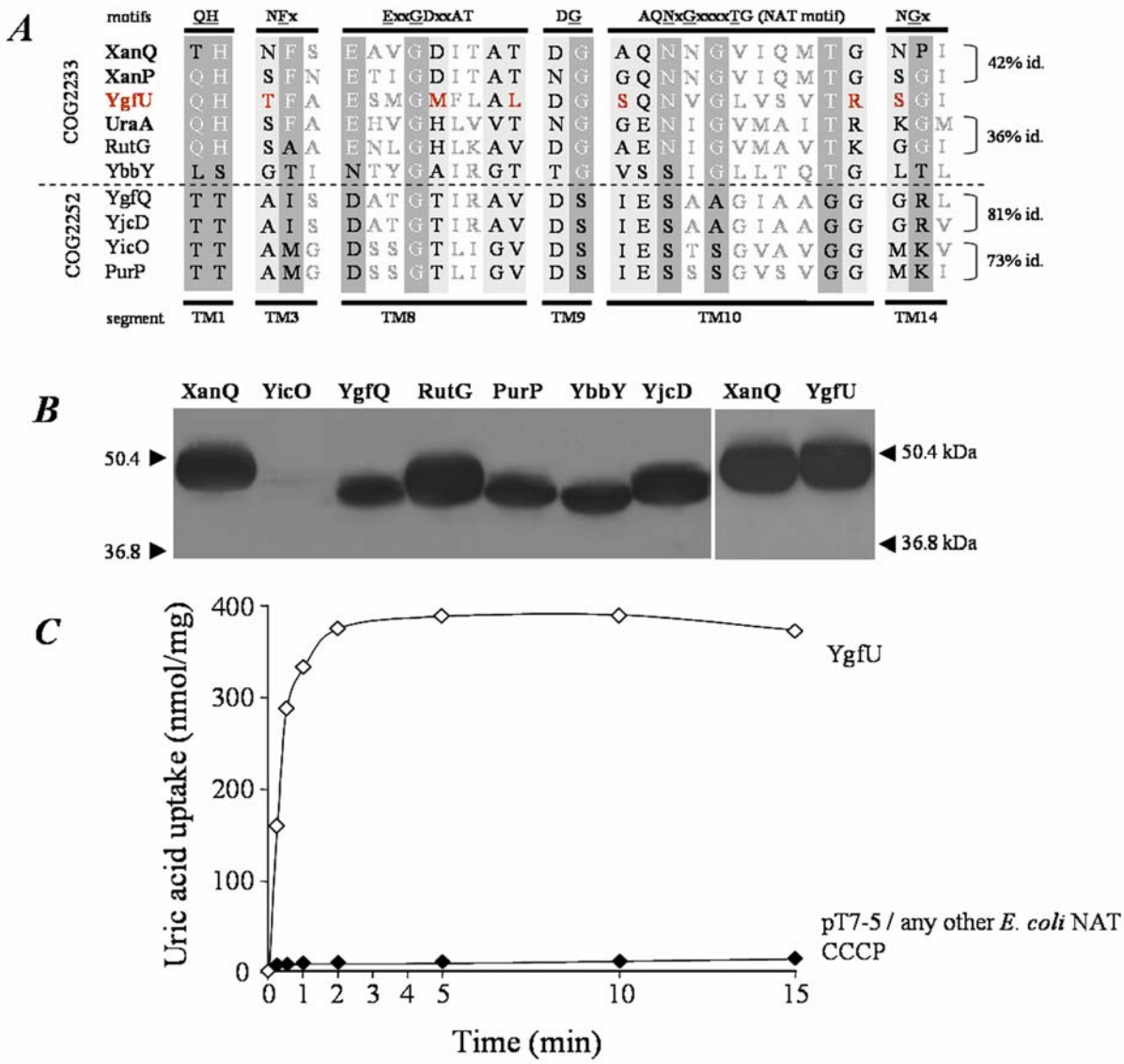

Figure 1

Downloaded from www.jbc.org at UNIVERSITY OF IOANNINA, on March 27, 2012

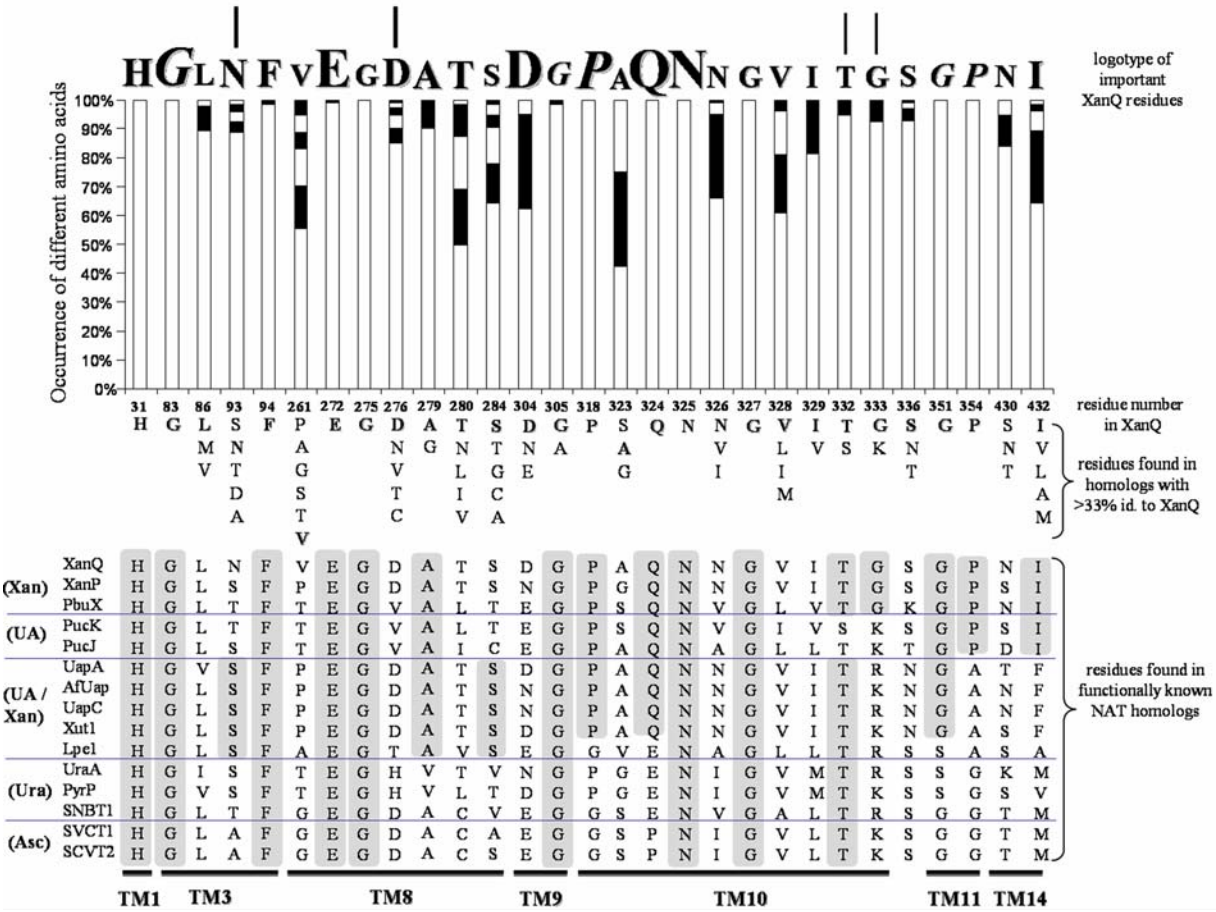

Figure 2

Downloaded from www.jbc.org at UNIVERSITY OF IOANNINA, on March 27, 2012

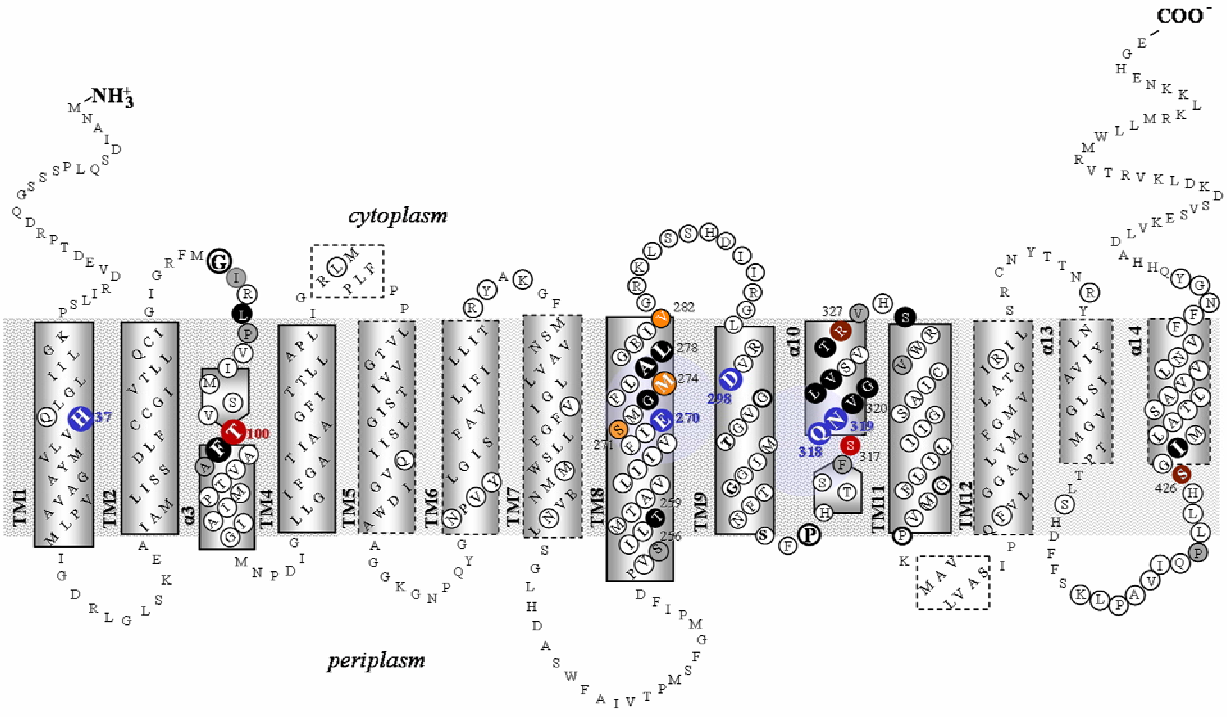

Figure 3

Downloaded from www.jbc.org at UNIVERSITY OF IOANNINA, on March 27, 2012

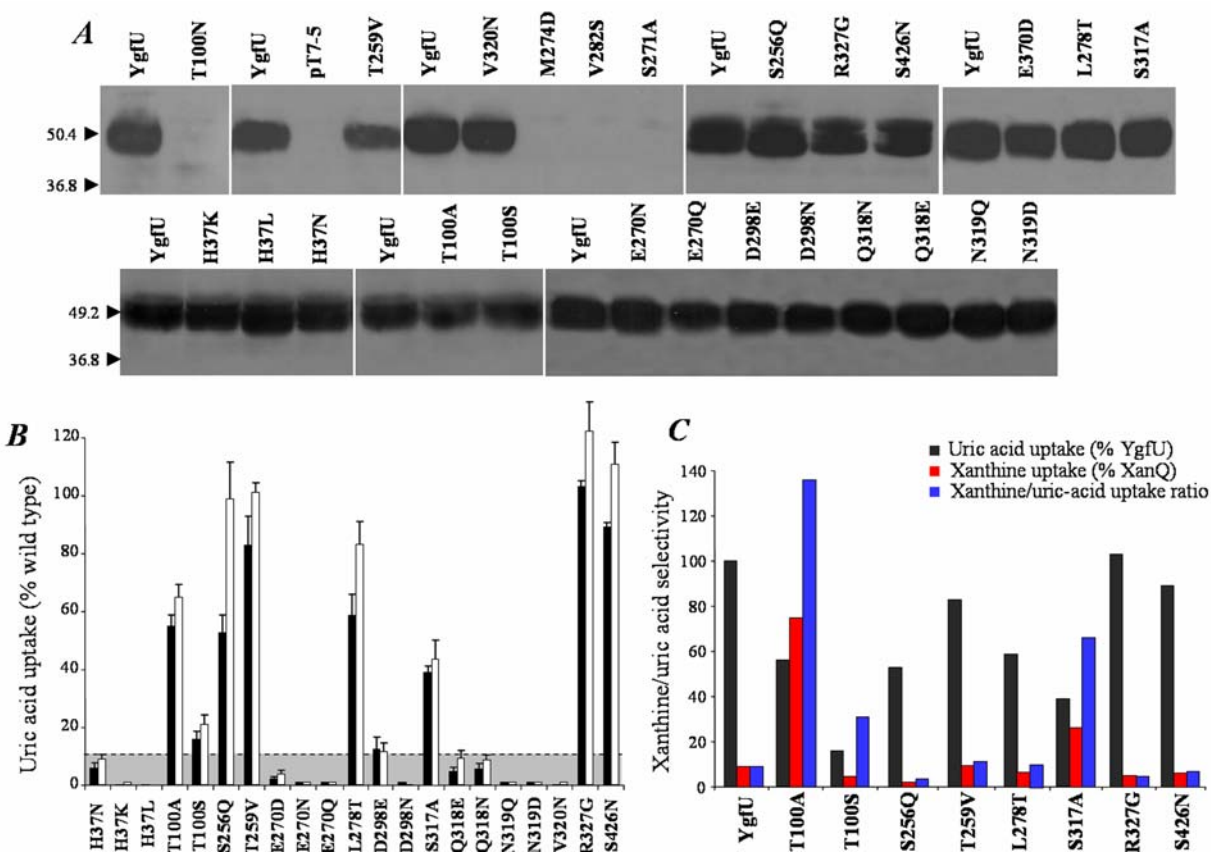

Figure 4

Downloaded from www.jbc.org at UNIVERSITY OF IOANNINA, on March 27, 2012

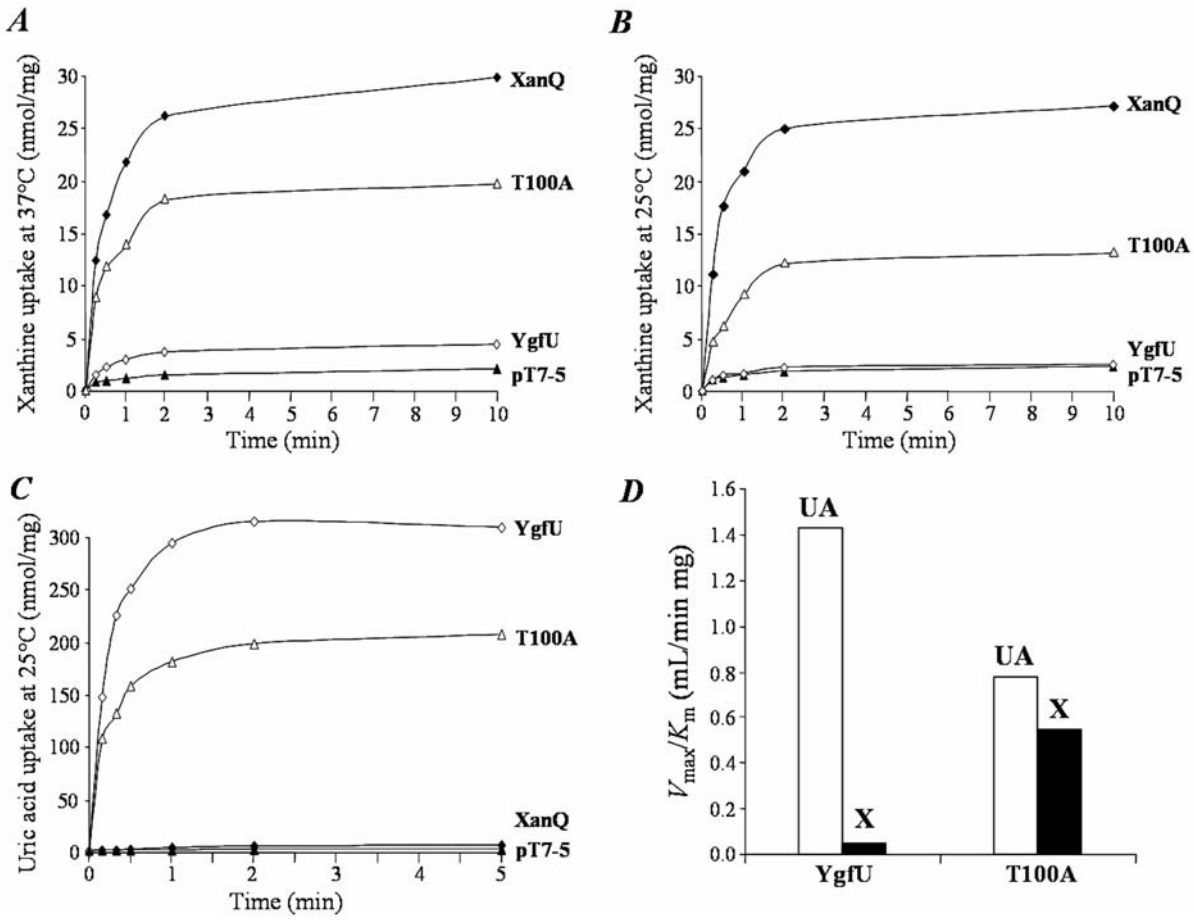

Figure 5

Downloaded from www.jbc.org at UNIVERSITY OF IOANNINA, on March 27, 2012

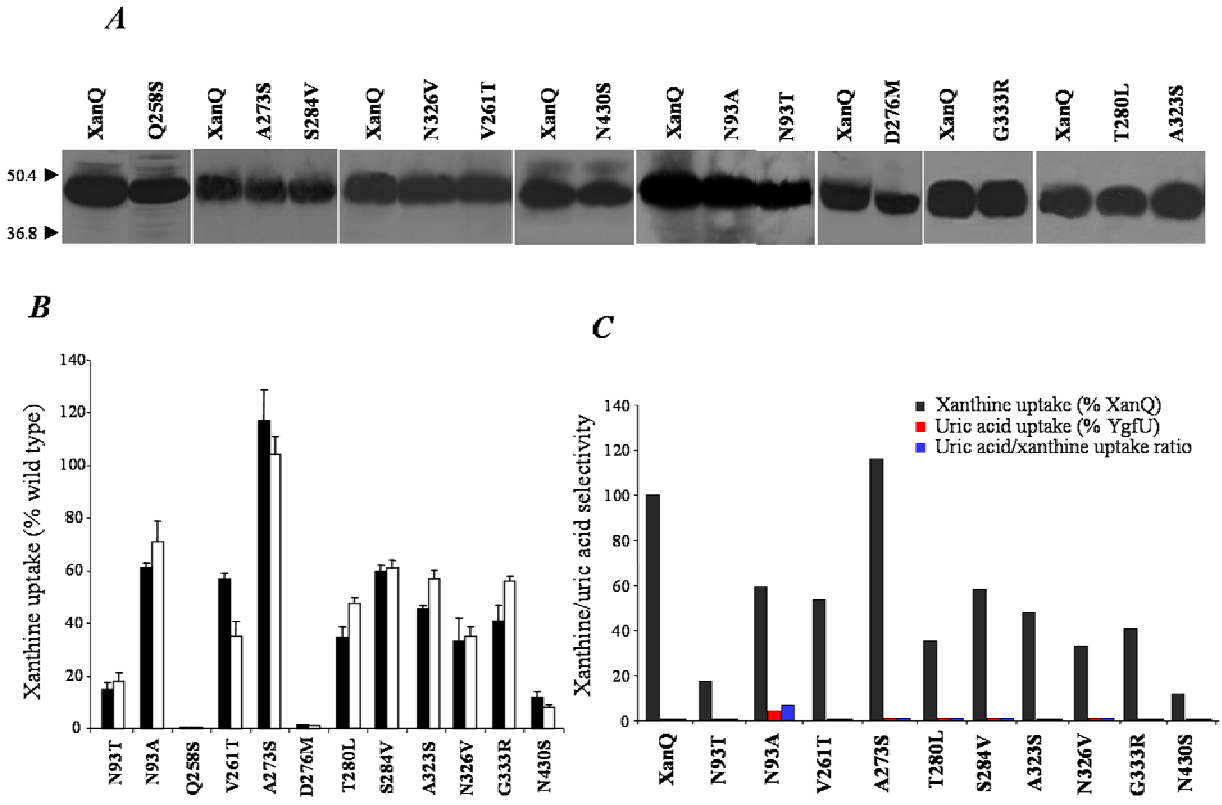

Figure 6

Downloaded from www.jbc.org at UNIVERSITY OF IOANNINA, on March 27, 2012

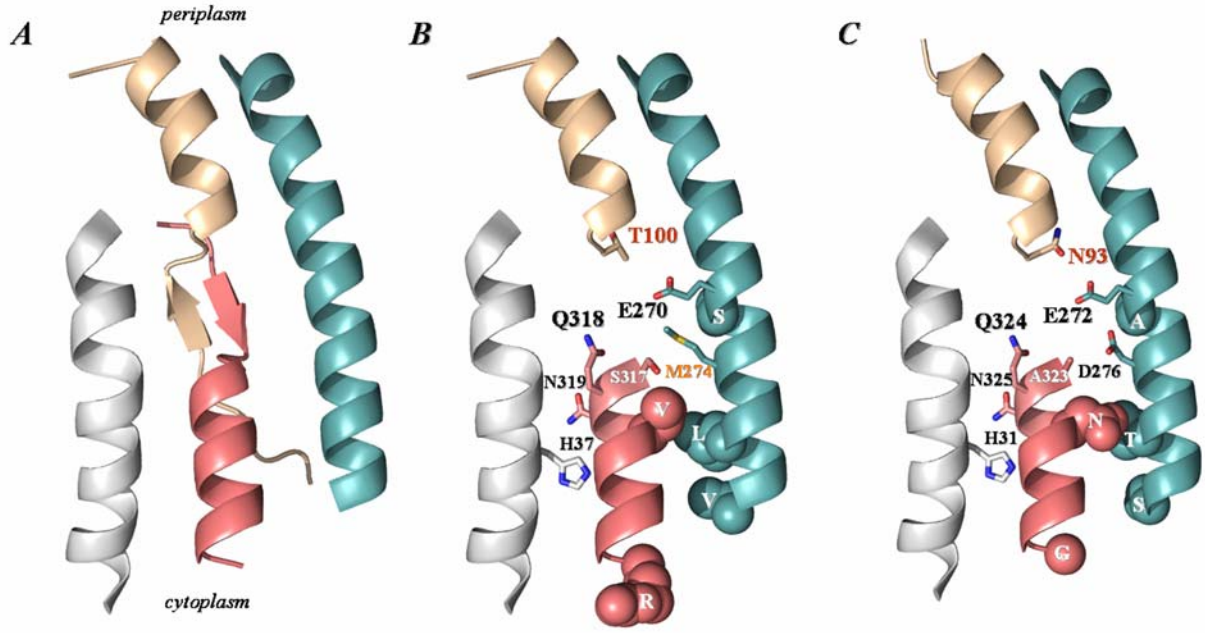

Figure 7

Downloaded from www.jbc.org at UNIVERSITY OF IOANNINA, on March 27, 2012